IAEA
International Atomic Energy Agency

20th IAEA Fusion Energy Conference
Vilamoura, Portugal, 1 to 6 November 2004

IAEA-CN-116/EX/P4-10

EXPERIMENTAL TEST OF NEOCLASSICAL THEORY OF POLOIDAL ROTATION IN TOKAMAKS

W.M. SOLOMON[1], K.H. BURRELL, L.R. BAYLOR[2], R.J. FONCK[3], P. GOHIL, D.J. GUPTA[3], R.J. GROEBNER, G.J. KRAMER[1], G.R. MCKEE[3], and R. NAZIKIAN[1]

General Atomics
San Diego, California 92186-5608
United States of America

[1]Princeton Plasma Physics Laboratory, Princeton, New Jersey, USA
[2]Oak Ridge National Laboratory, Oak Ridge, Tennessee, USA
[3]University of Wisconsin, Madison, Wisconsin, USA

Experimental Test of Neoclassical Theory of Poloidal Rotation in Tokamaks

W.M. Solomon 1), K.H. Burrell 2), L.R. Baylor 3), R.J. Fonck 4), P. Gohil 2), D.J. Gupta 4), R.J. Groebner 2), G.J. Kramer 1), G.R. McKee 4), R. Nazikian 1)

1) Princeton Plasma Physics Laboratory, Princeton, New Jersey, USA
2) General Atomics, San Diego, California, USA
3) Oak Ridge National Laboratory, Oak Ridge, Tennessee, USA
4) University of Wisconsin, Madison, Wisconsin, USA

e-mail contact of main author: wsolomon@pppl.gov

Abstract. The neoclassical theory of poloidal rotation is tested by comparing measured poloidal rotation profiles with predictions from the code NCLASS. This comparison is possible due to recent improvements in analysis techniques for charge exchange recombination spectroscopy measurements. Considerable effort has been spent to account for the systematic atomic physics corrections that play a significant role in the interpretation of both toroidal and poloidal rotation. After taking care of the atomic physics corrections, we find an order of magnitude discrepancy between the measured poloidal rotation and the neoclassical prediction from NCLASS. Moreover, the rotation is predicted to be in the opposite direction than what is actually observed. Confirmation of the accuracy of the experimental result is achieved through analysis of a different C VI transition.

1. Introduction

Rotation plays an important role in the suppression of turbulence and the formation of internal transport barriers through $E \times B$ shear. It is also involved in the stabilization of both resistive wall modes and neoclassical tearing modes. However, momentum confinement remains a poorly understood topic in fusion plasmas. Neoclassical theory allows predictions to be made about poloidal rotation. While neoclassical theory has been successful in predicting the magnitude of bootstrap current and the associated neoclassical resistivity in experiments, there has not been much success in predicting the cross-field transport of momentum. In order to achieve predictive knowledge of rotation, experimental verification of the neoclassical theory of rotation is required. Since the calculation of bootstrap current comes from the same order in the neoclassical theory as the poloidal rotation, such a comparison will also provide additional understanding of bootstrap current, which is essential for advanced tokamak scenarios.

The neoclassical theory of rotation is tested by comparing the poloidal rotation profiles from charge exchange recombination (CER) measurements [1-2] with predictions from the code NCLASS [3], which calculates the neoclassical transport properties of a multi-species plasma. Special care is necessary to properly interpret the CER measurements and ensure the comparison meaningful.

2. Measurement of Poloidal Velocity using Charge Exchange Recombination Spectroscopy

The determination of plasma rotation from charge exchange measurements is complicated by various atomic physics effects. The corrections due to the atomic physics can be substantial; for toroidal rotation, corrections up to 25% are common on DIII-D, and poloidal rotation can have corrections of order one. The fundamental problem occurs as a result of the energy dependence of the charge exchange cross section [4]. In particular, due to the finite ion temperature, some ions will experience a larger cross-section than others. Spectroscopically, one side of the emission profile is enhanced, while the other is diminished. This is equivalent to the Doppler shift in the line position due to rotation, and this apparent shift scales with ion temperature. Views that are perpendicular to the motion of the beam ions do not directly experience this effect. Since neutral beams are usually directed horizontally across the midplane of the tokamak vessel, one might be tempted to conclude that only the toroidal measurement of rotation is affected by the energy-dependence of the cross-section.

However, the measurement is further complicated by the fact that the excited state after charge exchange has a finite lifetime before emitting a photon. Coupled with the gyro-motion of the ions, the distortion of the lineshape due to the energy-dependent cross-section correction can precess into the vertical viewing direction, and hence affect poloidal rotation measurements [5]. In DIII-D, where the neoclassically predicted poloidal rotation is generally less than 1–2 km/s, the gyro-orbit correction in principle can be several times greater than this. Hence, it is vital to accurately handle the atomic physics corrections for the vertical views also if one is to undertake a worthwhile comparison with theory.

In addition, other effects must be accounted for when extracting poloidal rotation from the vertical views. Simple geometry considerations can have a significant impact on the interpretation of the measurements. Vertical views require that the spatial averaging of the chords be properly handled (for example, see Ref. [6]). Their measured velocities must also be adjusted to account for the fact that in reality the views may contain some toroidal component. With the toroidal rotation generally outranking the poloidal rotation by an order of magnitude, this in itself can be a substantial offset.

Previous efforts to handle the gyro-orbit correction on TFTR [5] have concentrated on using extensive and complicated atomic physics calculations to model the effective lifetime of the excited state. The difficulty with this approach lies with the uncertainties in the various cross-sections. The modeling results could explain some of the differences observed between opposing pairs of viewing chords, but ultimately it did not reconcile all the discrepancies, which tended to worsen with increasing toroidal rotation.

An alternate approach has been implemented at DIII-D to deal with the atomic physics corrections. By making use of vertical chords close to the magnetic axis, it is possible to determine the gyro-orbit correction directly from the measurements [7]. Such chords measure only atomic physics corrections, since there is effectively no poloidal velocity near the axis. Using this method alleviates the need to perform difficult atomic physics calculations. With the set of views utilized on DIII-D, it is also possible to verify the charge exchange cross section itself by making use of radial views through the plasma [7].

The plasma rotation is modeled using the neoclassical flux surface quantities $k(\rho)$ and $\Omega(\rho)$

$$\vec{V} = k\vec{B} + R\Omega\hat{\phi} \quad , \tag{1}$$

where R is the major radius, and $\hat{\phi}$ is the unit toroidal vector. In our analysis, the profiles of $k(\rho)$ and $\Omega(\rho)$ are represented by cubic splines [7]. Given k and Ω profiles, and the effective lifetime τ, the plasma rotation can be re-projected back into line-of-sight velocities using the actual viewing geometry. A non-linear least squares fitter minimizes the residuals between the measured line of sight (LOS) velocities and the re-projected values from the fit model by adjusting the knot locations and values of k and Ω, as well as solving for the effective lifetime τ.

3. Comparison of Measurement with Theoretical Predictions

The results presented in this paper concentrate on experiments performed in quiescent H-mode (QH-mode) discharges on DIII-D [8]. This mode of operation is of general interest, particularly because of the good plasma performance in the absence of edge localized modes (ELMs). QH-modes are of exceptional value for CER analysis, because the long steady phase without ELMs or sawteeth allows multiple, near-identical time slices to be analyzed and averaged to improve the statistics. This is particularly important for doing the detailed comparison of neoclassical theory presented here. The inherently high ion temperature observed in QH-mode ($T_i \geq 10$—15 keV) makes it a regime where it is important to take account of the atomic physics corrections.

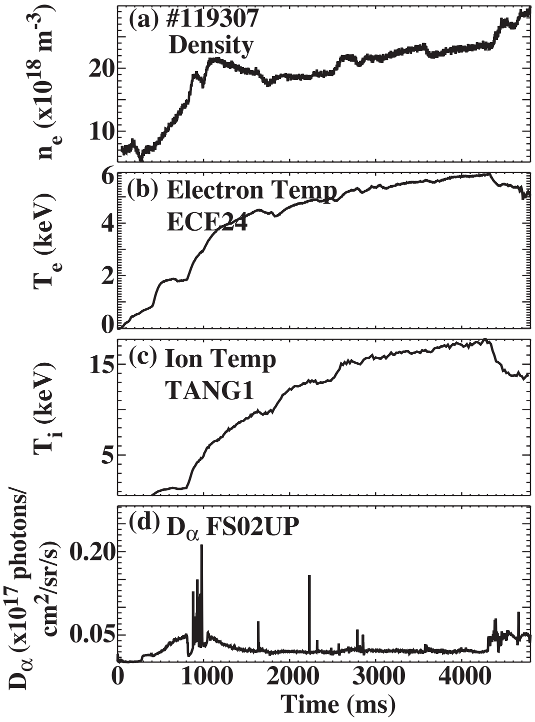

FIG. 1. Sample plasma parameters for #119307: (a) line average electron density, (b) central electron temperature, (c) central ion temperature, (d) D_α.

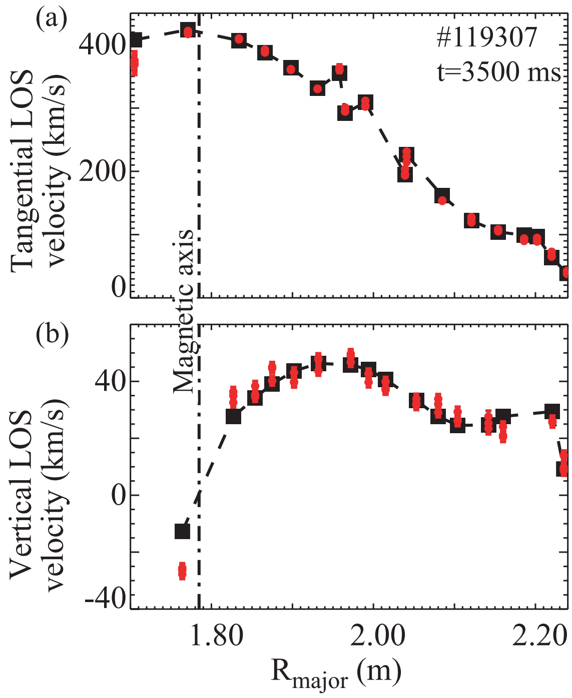

FIG. 2 Measured LOS velocities for (a) tangential and (b) vertical viewing CER chords. The red points are the measured values with error bars, while the black squares are the re-projected LOS velocities after solving for k, Ω, and τ. The jaggedness in the tangential profile arises due to the fact that the chords are viewing the plasma from two distinct ports, and consequently have different toroidal angles.

Figure 1 shows the time evolution of the line average density, central electron and ion temperatures and D_α signal for shot #119307. One can see that during the quiescent phase from 1800 ms onwards, there are only a few bursts of ELM activity. CER data was acquired at the C VI (8–7) line at 529.05 nm, with 10 ms integration time. The neutral beams were modulated, which gives significantly cleaner charge exchange spectra when combined with time slice subtraction. This works particularly well in QH-mode, generally leaving only a single Gaussian fit, which greatly simplifies and improves the CERFIT spectral analysis.

The measured LOS velocities from the tangential and vertical viewing chords are shown in Fig. 2 for a particular time slice during the QH-phase. The red points represent the measured data with error bars, and the black squares are the re-projected LOS velocities after solving for the fit parameters k, Ω, and τ. With four knots in each of k and Ω, we are able to achieve a reasonable fit to the data. Note in particular that the innermost vertical channel is inside of the magnetic axis, R_0. As such, the contribution of the poloidal velocity changes sign for this chord. On the other hand, the contribution of the gyro-orbit correction remains constant across the magnetic axis. Therefore, the gyro-orbit correction effectively opposes the poloidal rotation in the measured LOS velocity for $R>R_0$, and reinforces it inside of the magnetic axis.

The toroidal velocity profile from C VI, corrected for the energy-dependent cross section, is shown in Fig. 3. Although the toroidal velocity is not a flux function, it is plotted against ρ, specifically, along the outer midplane. The rather high central velocity of more than 500 km/s is typical for QH-mode discharges. For comparison, the uncorrected profile is also plotted. The correction results in a 25% (>100 km/s) increase to the inferred central rotation. Confidence in the toroidal rotation measurements is provided through a cross-comparison between two tangential chords (T5 and T20) that view the same spatial location, but with slightly differing viewing geometries. The raw measured velocities as a function of time are shown in Fig. 4(a). The two measurements clearly do not agree. A small offset of about 5% is expected based on the difference between the toroidal angles of the two views. However, the discrepancy

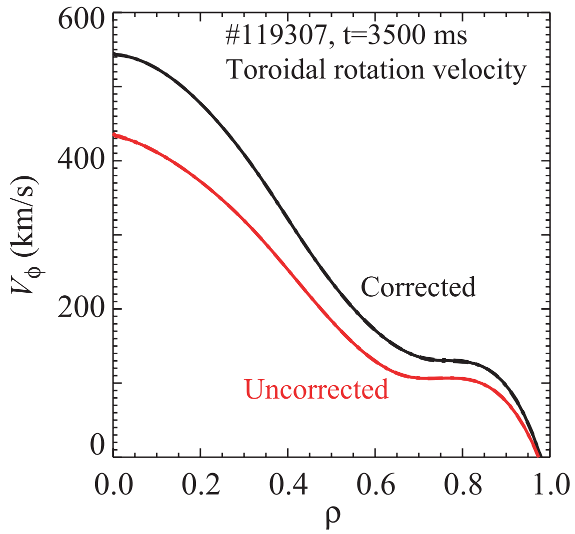

FIG. 3. Toroidal velocity profiles, corrected (black) and uncorrected (red) for the energy-dependent cross-section correction.

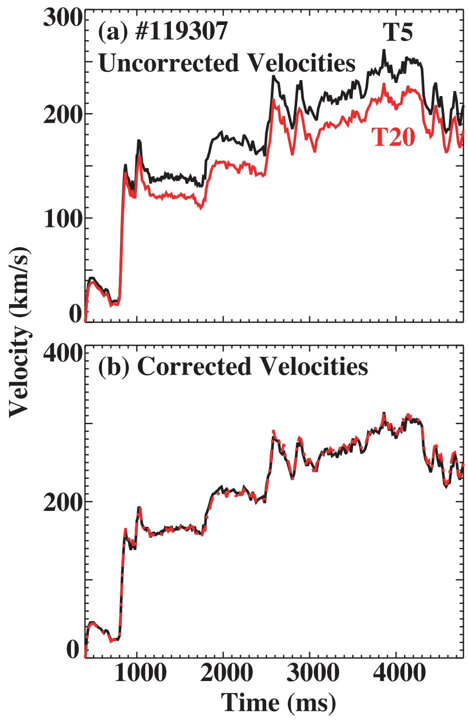

FIG. 4. Comparison of two tangential chords viewing the same spatial location, but with slightly differing viewing angles. (a) Uncorrected and (b) corrected for the energy-dependent cross-section correction.

between the measurements is notably greater than this. In fact, the dissimilarity can be traced to the energy dependent cross-section correction. After applying this correction, the two measurements snap together with near perfect agreement [Fig. 4(b)].

Shown in Fig. 5 is the fully corrected poloidal velocity profile. As with the toroidal velocity, the poloidal rotation velocity is also not a flux surface function, but again is plotted here against ρ along the outer midplane. Individual time slices have been analyzed and the result displayed is the time average over the window t=[3000–4000] ms. The error bands are the standard deviation of the time resolved profiles. Note that most of the error estimate can be attributed to the variation in the measurement at different times. In principle, some of the error is due to instability in the spline fitting technique, although this is largely mitigated by fixing the knot locations of k and Ω. The poloidal rotation is positive everywhere across the profile, which is in the direction of the ion diamagnetic drift, and physically points downwards along the outer midplane.

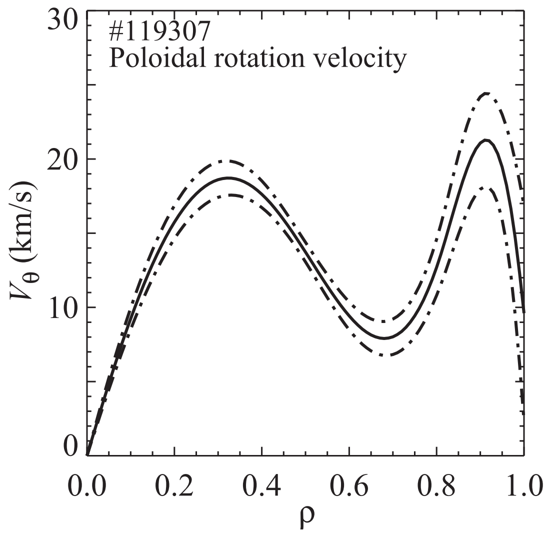

FIG. 5. Measured poloidal rotation velocity for #119307. The solid curve represents the time average of multiple time slices between t=[3000, 4000] ms. The dashed curves represent the error bands, which are shown as the one standard deviation of the individual time slices in this period.

The measured poloidal velocity profile is compared with the neoclassical prediction from the code NCLASS. Actual plasma profiles of the electron temperature, electron density, ion temperature, carbon impurity density, and (corrected) toroidal velocity for the discharge are input into NCLASS through a front-end code FORCEBAL,which computes the radial force balance. The NCLASS prediction of the poloidal velocity is shown in Fig. 6(a). Again, the profile is obtained by averaging multiple time slices over the time window [3000, 4000] ms and the dashed error bands represent the standard deviation of the profiles in this analysis window.

It is immediately apparent that the NCLASS prediction is smaller by an order of magnitude compared with the experimental observation, illustrated more clearly when plotted together on the same scale in Fig. 6(b). Equally surprising, there is even disagreement in the ***direction*** of the rotation between the two profiles. While the predicted poloidal velocity of carbon from NCLASS seems inconsistent with the measurements, an interesting observation is that the predicted ***deuterium*** poloidal rotation shows curious agreement with the carbon measurement, both in magnitude and in direction. It is worth noting that the region in the plasma (ρ~0.3) where the discrepancy is most pronounced between the measured poloidal rotation velocity and the neoclassical prediction corresponds to the region where the fit to the data shown in Fig. 2 is particularly good (1.9<R (m) <2.0). Accordingly, the minor discrepancies between the data and the fit in Fig. 2 close to the axis are unlikely to play any role in the marked deviation of the measured poloidal rotation from the neoclassical prediction.

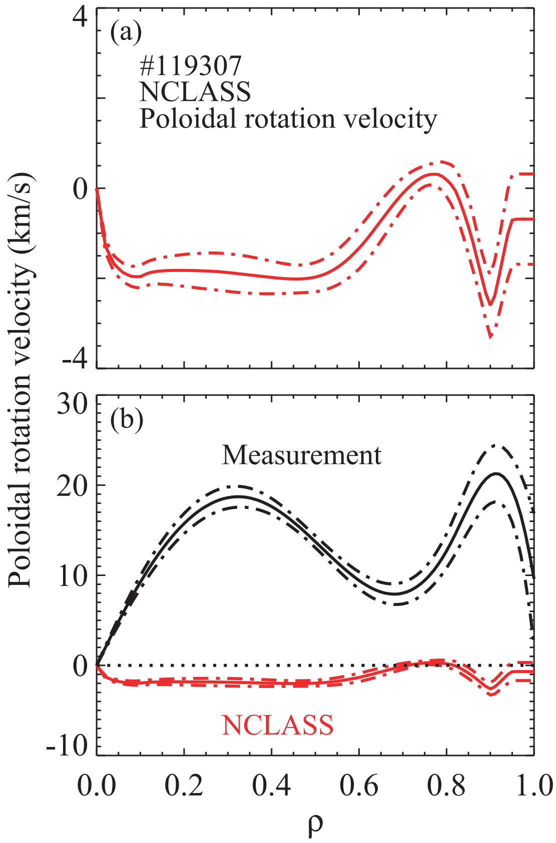

FIG. 6. (a) Neoclassically predicted poloidal velocity as determined by the code NCLASS. (b) For clarity, the measured and theoretical poloidal rotations plotted on the same axes.

3.1 Verification of Measurement Techniques

Despite the rigorous attention we have devoted to properly accounting for all the physics affecting the interpretation of the poloidal rotation, the intrinsic complexity of the measurement warrants a method of verifying the result. To this end, we utilized the flexibility of the DIII-D CER system and performed the measurement on a nominal repeat shot with the system tuned to the C VI (7–6) transition at 343.37 nm. The advantage of this approach is that the atomic physics corrections (both energy-dependent cross-section, and gyro-orbit) will be different at this alternate wavelength. Hence, if we can find good agreement between the two data sets, then we will have additional confidence in our interpretation of the measurements.

The time evolution of two shots, #119306 and #119307, is shown in Fig. 7 for the line average density, central electron temperature and central ion temperature, over the quiescent phase of interest. The reproducibility is very good (although in the earlier time phase (not shown) there is some discrepancy in density).

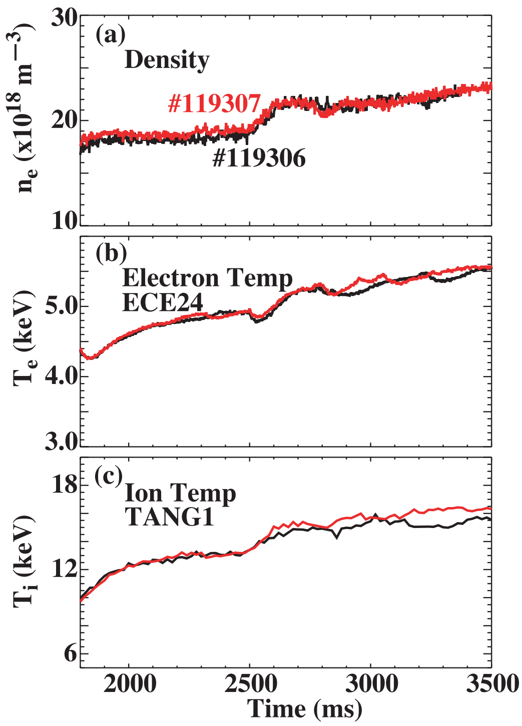

FIG. 7. Time evolution comparison during the quiescent phases of #119306 (black) and #119307 (red) (a) line average density, (b) central electron temperature, (c) central ion temperature.

Actually, it was not possible to tune ***all*** the CER channels to the desired (7–6) wavelength. Presently, some of the vertical chords are connected to older intensified photodiode detectors (as opposed to the majority of chords that use modern CCD's), which are not sensitive down to this wavelength. The clear disadvantage to this limitation is that we do not have the optimal number of vertical views to best determine the poloidal rotation profile (as described in Ref. 7). However, it is beneficial to retain some chords viewing the normal (8–7) transition as a check that the poloidal velocity profile is consistent across the two shots. Essentially, we can extract two independent (albeit less accurate) poloidal rotation profiles by using the two different sets of wavelength measurements. If we are properly accounting for the atomic physics, then the two profiles should agree.

The inferred profiles from the two wavelengths are shown in Fig. 8. Although the agreement between the profiles is not perfect, it is acceptable, especially considering that both profiles come from incomplete sets. In any case, the neoclassical prediction disagrees markedly with both poloidal velocity profiles.

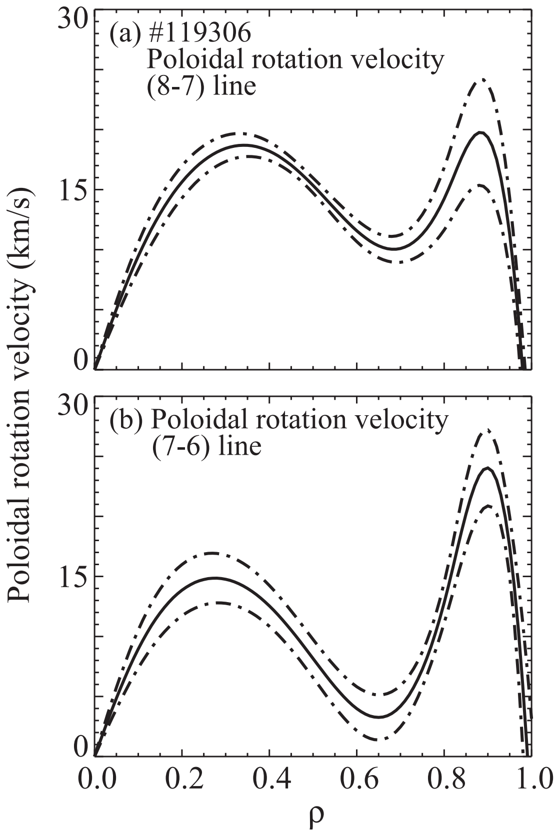

FIG. 8. Inferred poloidal velocity profiles for #119306 using vertical chords tuned to (a) C VI (8–7) line, 529.05 nm, and (b) C VI (7–6) line, 343.37 nm.

3.2 Consequences for Radial Electric Field Determination

The order of magnitude difference observed between the measured and NCLASS predicted poloidal rotation has an interesting impact on the radial electric field determination. In Figure 9, the total radial electric field E_r is shown, using the poloidal rotation as determined from (a) the measurements and (b) the neoclassical prediction. It is clear that there is a marked difference in the result depending on whether one uses the measured or theoretical poloidal rotation in calculating E_r. Given the importance of the radial electric field to plasma confinement, in terms of turbulence suppression and transport barrier formation through $E\times B$ shear stabilization, it is essential to be able to accurately determine E_r.

It is possible to indirectly examine E_r by looking at the poloidal propagation velocity of the turbulence, V_θ^{fl}. The radial electric field is estimated by assuming that the fluctuations propagate with the $E\times B$ drift velocity, so that $V_\theta^{fl} = E_r/B_\phi$, where B_ϕ is the toroidal magnetic field. This approximation is good in most conditions in DIII-D, although it may be violated close to the plasma edge, where diamagnetic velocities can become comparable to the $E\times B$ poloidal velocity. The recently upgraded beam emission spectroscopy (BES) diagnostic [9] can measure a time delay between two poloidally separated channels measuring density fluctuations deep in the core plasma. This time delay is then used to determine V_θ^{fl} [10]. Unfortunately, the magnetic field pitch angle in QH mode discharges is of the opposite sign than usual in DIII-D due to the reversed plasma current. This results in poorer alignment of the BES sightlines to the magnetic field lines, which are optimized for normal operation, and in turn reduces the poloidal wavenumber sensitivity. Nevertheless, the low-k fluctuations are still observable with the enhanced-sensitivity BES system now available on DIII-D. The radial locations of the BES channels were scanned over a series of nominally similar shots starting with #119311.

The inferred propagation velocity is shown in Fig. 10. Overplotted is the corresponding E_r/B_ϕ measurement from CER. Two curves are shown, differing in the choice of the poloidal rotation. The black curve uses the experimentally determined poloidal rotation profile, whereas the red curve assumes the neoclassically predicted profile. The BES measurements are more consistent with E_r calculated from the experimental poloidal velocity.

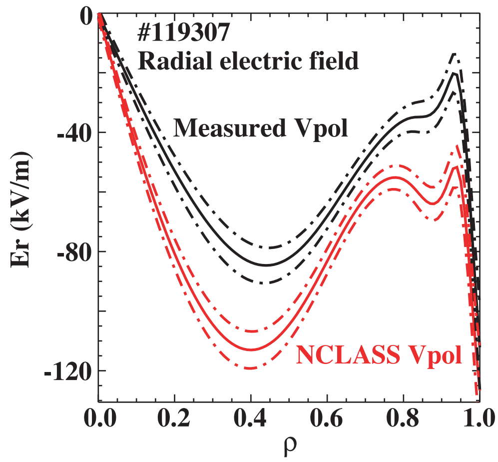

FIG. 9. Radial electric field profiles, using the poloidal velocity as determined by measurement (black) and theory (red).

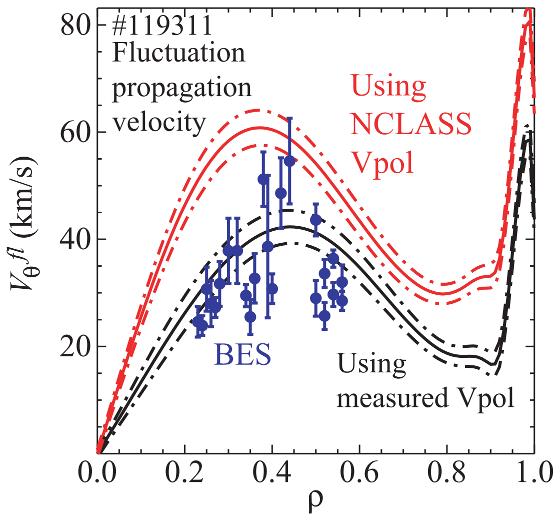

FIG. 10. Comparison of the poloidal propagation velocity of the turbulence as measured by the time delay method with the BES diagnostic. The various radial locations are obtained from a series of nominally similar discharges. Two profiles of E_r/B_ϕ from CER are plotted. The black curve uses the experimentally measured poloidal velocity, while the red curve substitutes the NCLASS prediction.

4. Discussion

While significant differences between the experimentally measured poloidal velocity and the neoclassical theory predictions have been reported before, those measurements were made at the transport barriers with steep pressure gradients at the DIII-D H-mode edge [11] and at the TFTR enhanced reverse shear (ERS) [12]. It is expected that the neoclassical prediction could be unreliable when the ion pressure gradient scale length is comparable to the ion gyro-radius for poloidal magnetic field, $L_p \sim \rho_{i\theta}$, as was encountered in those experiments. In this respect, the degree of discrepancy in Fig. 6 is remarkable, since in these QH-mode discharges the profiles do not exhibit steep gradients, except near the last closed flux surface.

The cause for the apparent anomalous poloidal rotation is at this stage not clear. One possibility relates to the effects of fast ions. The neutral beam injection is capable of driving a parallel flow, through the friction between the fast ions and the thermal population. At present, this parallel drive is not incorporated into NCLASS, although an upgrade is in progress [13]. Once the fast ion terms are included in the parallel force balance, we will be able to assess the contribution of this effect.

The anomalous poloidal rotation may also be generated through core turbulence. In particular, the turbulent Reynolds stress has been theoretically predicted [14] and demonstrated experimentally [15–16] as a mechanism for generating poloidal flow.

A recent code, GTC-Neo, performs global kinetic particle simulation to calculate the neoclassical transport coefficients and equilibrium radial electric field. It includes finite orbit effects and a systematic treatment of rotation. Simulations of plasmas with large toroidal rotation and strong shear are found to drive poloidal rotations (of the main ion species) up to a factor of two greater than neoclassical theory [17]. This result may be of relevance to the rapidly rotating QH-mode plasmas. However, the code does not presently incorporate impurities, and so the result cannot be directly applied.

In summary, we have made unprecedented efforts to ensure that the interpretation of the poloidal rotation from CER measurements is as accurate as possible. Even after taking care of all the atomic physics corrections, we still find an order of magnitude discrepancy between the measured poloidal rotation velocity and the neoclassical prediction from NCLASS. Additionally, the direction of the rotation is not even the same. New physics understanding is necessary to reconcile these differences. Future experiments with scans in key parameters such as the ion temperature gradient should be productive in determining any systematic trends and anomalies between theory and measurement.

Acknowledgments

This work is supported by US DOE under Cooperative Agreement No. DE-FC02-04ER54698 and Contract Nos. DE-AC02-76CH03073, DE-AC05-00OR22725, DE-FG03-96ER54373, and DE-FG03-01ER54615.

References

[1] BURRELL, K.H., *et al.*, Rev. Sci. Instrum. **72** (2001) 1028.
[2] BURRELL, K.H., *et al.*, Rev. Sci. Instrum., *in press*.
[3] HOULBERG, W.A., *et al.*, Phys. Plasmas **4** (1997) 3230..
[4] VON HELLERMAN, M., *et al.*, Plasma Phys. Control. Fusion **37** (1995) 71.
[5] BELL R.E., and SYNAKOWSKI, E.J., AIP Conf. Proc. **547** (2000) 39.
[6] BELL, R.E., Rev. Sci. Instrum. **68** (1997) 1273.
[7] SOLOMON, W.M., *et al.*, Rev. Sci. Instrum, *in press*.
[8] BURRELL, K.H., *et al.*, Phys Plasmas **8** (2001) 2153.
[9] GUPTA, D.K., *et al.*, Rev. Sci. Instrum., *in press*.
[10] DURST, R.D., *et al.*, Rev. Sci. Instrum. **63** (1992) 4907.
[11] KIM, J., *et al.*, Phys. Rev. Lett. **72** (1994) 2199.
[12] BELL, R.E., *et al.*, Phys. Rev. Lett. **81** (1998) 1429.
[13] HOULBERG, W., *et al.*, to be presented at APS conference, Savannah GA (2004).
[14] DIAMOND P.H., and Y.B. Kim, Phys Fluids B **3** (1991) 1626.
[15] HIDALGO, C., *et al.*, Phys. Rev. Lett. **83** (1999) 2203.
[16] MOYER, R.A., *et al.*, Phys. Rev. Lett. **87** (2001) 135001.
[17] WANG, W.X., *et al.*, presented at Sherwood Fusion Theory conference, Rochester NY (2002).